PFC/JA-93-16

Electron Distribution Function Measurements on a Magnetron Injection Gun Beam

W.C. Guss, M.A. Basten, K.E. Kreischer, and R.J. Temkin

July 1993

Plasma Fusion Center
Massachusetts Institute of Technology
Cambridge, MA 02139-4294 USA

This work was supported by Department of Energy Contract No. DE-AC02-78ET51013

Submitted for publication in *Journal of Applied Physics*.

Electron Distribution Function Measurements on a Magnetron Injection Gun Beam

W.C. Guss, M.A. Basten, K.E. Kreischer, and R.J. Temkin

Plasma Fusion Center
Massachusetts Institute of Technology

Abstract

The parallel electron distribution function has been measured on an electron beam from a magnetron injection gun (MIG) using an $E \parallel B$ energy analyzer. The magnetic field, beam voltage and beam current were scaled down from normal operating parameters. The perpendicular velocity spread, inferred under the assumption that the electrons are mono-energetic, is relatively constant for electron velocity ratios $\beta_\perp/\beta_\parallel > 0.7$ and increases approximately linearly with the beam current. The current scaling of the perpendicular velocity spread is also consistent with electron loss currents measured at the control anode of the MIG. Observed perpendicular velocity spreads for the gun design parameters are substantially larger than computational values.

PACS Nos. 41.80.Dd, 52.75.Ms, 29.25.Bx

Introduction

Recent high power, high frequency gyrotron measurements[1] have shown discrepancies between the observed values and efficiency estimates from a single-mode self-consistent nonlinear code with the velocity ratio fixed at its design value. It was also observed that the optimum and maximum obtainable velocity ratio, $\langle\alpha\rangle = \langle v_\perp\rangle/\langle v_\parallel\rangle$, where $v_\perp$ and $v_\parallel$ are the electron velocity components perpendicular and parallel to the magnetic field, generally decreased as a function of increasing electron beam current. Introducing the experimentally observed $\langle\alpha\rangle$ values into the computational model reduced the calculated efficiency, and also the difference between the calculated and experimental results, but did not fully eliminate it. The observed operational limit for obtainable values of $\langle\alpha\rangle$, and therefore the efficiency, at beam currents $I_b \geq 20\,A$ resulted from erratic behavior of the electron beam and arcing. The arcing appeared to be in the vicinity of the electron gun and was believed to be a result of electrons mirrored by the cavity magnetic field. Under optimum conditions, the mean velocity of all the beam electrons would prevent mirroring. However, if the velocity spread is sufficiently large then some small fraction of the beam will mirror.

In addition to an operational limit on $\langle\alpha\rangle$, there are effects on the efficiency at a given $\langle\alpha\rangle$ resulting from spreads in the perpendicular velocity of the beam electrons. Gyrotrons operate with large perpendicular wavenumber ($k_\perp \approx k$, where k is the vacuum wavenumber) and a much smaller parallel wavenumber ($k_\parallel << k$). As a consequence of the Doppler shift criterion for the frequency, $\omega = k_\parallel v_\parallel + \Omega_e/\gamma_o$, and the ordering $\omega \approx \Omega_e/\gamma_o >> k_\parallel v_\parallel$, variations in $v_\parallel$ are generally regarded as having a small effect on the electron dynamics. Variations in $v_\perp$ have a larger effect because it interferes with the electron bunching process. Single-mode, nonlinear, self-consistent computer simulations of gyrotron efficiency have been performed for perpendicular velocity spreads ($\delta v_\perp/v_\perp \leq 10\%$) and have shown modest reductions in energy extraction efficiencies from the beam.

A measurement of the velocity distribution function would be required to assess the effect of the beam quality by either $\langle\alpha\rangle$ limiting or efficiency degradation from velocity spread. Measurements of the velocity spread have been performed by Avdoshin[2,3], Antakov[4], and Piosczyk[5]. The spreads in the Soviet literature[3], defined in terms of the retarding potential values where 10% and 90% of the current is collected, were large, in some cases near $\pm 20\%$ (or about $\pm 23\%$ RMS spreads). Surface roughness and thermal inhomogeneities were suggested as possible causes for these large spreads. The measurements were made in triode magnetron injection guns (MIG) which were operated at scaled down parameters[6]. Piosczyk[5]also reports large perpendicular velocity spreads ($\pm 30\%$ at $20\,A$) and also used a large scaling factor (20) for his reduction of beam voltage.

Previous measurements[7] were conducted with an $E \parallel B$ energy analyzer similar in design to that described below. The electrons were collected on the high voltage repelling electrode. These measurements were conducted at the design voltage ($80\,kV$) but at a reduced current of $I_b = 6\,A$ because of voltage breakdown problems within the diagnostic.

However, for these conditions, a full-width at half-maximum velocity spread of $\delta v_\perp / v_\perp \approx$ 10% FWHM ($\approx \pm 6\%$ RMS spread) was measured for $1.0 \leq \alpha \leq 2.0$. In this report, we describe results of operation with scaled parameters that extend our previous results.

Experimental Apparatus

Experiments were conducted in a $140\,GHz$ high power gyrotron[1] which consisted of an electron beam source, a magnetic mirror to convert electron parallel energy to perpendicular energy, and an open-ended resonant cavity as shown in Fig. 1. The electron beam was generated by a triode magnetron injection gun (MIG) which was designed[8] to operate at a beam voltage $V_b = 80\,kV$ and a beam current $I_b = 35\,A$ with a velocity ratio $\alpha = 1.93$. The computed perpendicular RMS velocity spread was $\pm 3.6\%$ for these parameters. The control-anode voltage during $80\,kV$ operation is $24.5 - 25.0\ kV$. The pulse length was $3\,\mu s$. The compression ratio $B_c/B_g \approx 30$, where B_c, and B_g are the magnetic fields at the cavity and the gun cathode, respectively. Typical gyrotron operation for varying $\langle\alpha\rangle$ was obtained by holding the control-anode voltage constant and varying the value of B_g. Efficient transport of the electron beam requires that all of the beam electrons enter the loss cone of this single ended mirror. At the design magnetic field (5.55 T) for $TE_{15,2}$ operation, the beam radius is $r_b = 0.53\,cm$.

The $E \parallel B$ energy analyzer is shown in Fig. 2 and uses a well known design[9,10]. The slotted disk is located at a position corresponding to the entrance of the gyrotron cavity, which has been removed for these measurements, and allows $\approx 5\%$ of the beam current to enter the diagnostic. The cylinder has a radius $r = 2r_b$ and a length $L = 8r_b$. High voltage is applied only to the cylinder and only those electrons with sufficient parallel energy reach the collecting electrode. This design has the advantage that any secondary electrons originating at the collecting electrode are returned to the electrode by the nearby high voltage cylinder. The magnetic field in this region is uniform to about 1% so there is no conversion of energy between velocity components in or near the diagnostic. Also shown in Fig. 2 is the location of a capacitive probe[11] used to measure $\langle v_\parallel \rangle$ and infer $\langle\alpha\rangle$. Its axial position near the normal cavity location ensures that the measured $\langle\alpha\rangle$ values are the same as those in the cavity, when present, or the energy analyzer in the present experiment.

Experimental Scaling

Previous experiments[7] performed at full cathode voltage and magnetic field, were limited to low beam current by arcing in the diagnostic. For the present experiments, the operating parameters were reduced in such a way that the beam radius and thickness matched full parameter operation. Keeping beam geometry constant relative to the cathode and accelerating electrodes implies the guiding center and cyclotron radius

$\rho_c = \gamma m_o v_\perp / eB_c$, where $\gamma = (1-\beta^2)^{-1/2} = 1 + eV_{ca}/m_o c^2$, remain constant. Here, e and m_o are the electron charge and rest mass, respectively. The perpendicular velocity of electrons near the cathode is well approximated[12] by the $E \times B$ velocity, where E is approximately $V_{ca}/\delta r_{ca}$, so that

$$\rho_c = \frac{m_o}{e\,\delta r_{ca}}(1 + \frac{eV_{ca}}{m_o c^2})\frac{V_{ca}}{B_c^2}$$
$$\approx \frac{\gamma V_{ca}}{B_c^2} .$$

V_{ca} and δr_{ca} are the cathode to control-anode voltage and radial separation. In addition, space charge effects near the cathode remain unchanged for $I_b/V_{ca}^{3/2}$ held constant. Consequently for a modest reduction of the cavity magnetic field $B_c = {}^1/_2 B_{co}$, then $V_{ca} \approx {}^1/_4 V_{cao}$ and $I_b \approx {}^1/_8 I_{bo}$ where the full parameter magnetic field, control-anode voltage and beam current are B_o, V_{cao}, and I_{bo}. Experimentally it was found that the same $\langle\alpha\rangle$ limiting behavior was observed at the scaled parameters as with the full parameters. Three values of scaled down current were selected, 1.95 A, 3.6 A, and 5.05 A which correspond to currents at normal voltage and magnetic field of about 15 A, 29 A, and 40 A, respectively.

Results

Data was taken for both dynamic and static bias voltages. For the dynamic voltage case, the high voltage repeller voltage was swept during the $\approx 2.5\mu s$ flat top of a single gyrotron pulse. An example of the voltage pulse with the resulting collector electrode current and baseline are shown in Fig. 3. The resultant current characteristic used for analysis was determined by subtracting the baseline from the net electrode current. To determine whether the baseline subtraction provided accurate curves, static voltages were also applied to the probe. In this case, data was taken with a constant voltage applied in steps to successive gyrotron pulses. The data from these two techniques are shown in Fig. 4 for the cases of low $\langle\alpha\rangle$ and high $\langle\alpha\rangle$ cases. The low $\langle\alpha\rangle$ case was investigated because of its rapid change in collected current which could include capacitive effects. The high $\langle\alpha\rangle$ case was investigated because of its relatively large noise level. In both cases however, the curves are similar and the fitted parallel velocity distributions are in good agreement. For the bulk of the results reported here, the dynamic voltage method was employed.

The experimental data was fitted using two techniques. If a Gaussian distribution is assumed for the parallel velocity, then the current reaching the collecting electrode I_p as a function of the retarding potential V_r can be described by

$$I_p(V_r) \propto e\int_{v_{\parallel r}}^{\infty} v_\parallel \exp[-(v_\parallel - v_{\parallel o})^2/\sigma^2]\,dv_\parallel$$
$$= \frac{I_{po}\left(\frac{\sigma}{\sqrt{\pi}}\exp[-(v_\parallel - v_{\parallel o})^2/\sigma^2] + v_{\parallel o}(1 - \mathrm{erf}[(v_{\parallel r} - v_{\parallel o})/\sigma])\right)}{\frac{\sigma}{\sqrt{\pi}}\exp[-(v_{\parallel o}/\sigma)^2] + v_{\parallel o}(1 + \mathrm{erf}[v_{\parallel o}/\sigma])} ,$$

where $v_{\|r} = \sqrt{2eV_r/m}$, and I_{po} is the current with no retarding potential, and erf(x) is the Error Function. Another approach is to fit a curve to the data and then take the derivative of the fitted curve. The velocity distribution function is then found using the expression

$$f(v_{\|r}) \propto \frac{1}{v_{\|r}} \frac{dI_p(v_{\|r})}{dv_{\|r}} .$$

The results for each of these approaches are illustrated in Fig. 5. The fit of either method gives the mean velocity $v_{\|o}$ and the RMS spread $\sigma = \delta v_{\|}$. Using the assumption that the energy spread is negligible, $v_{\perp o}$ and thus $\langle\alpha\rangle$ can then be calculated. The quality of the fit is determined by comparing the experimentally determined velocity ratio from the capacitive probe to the $\langle\alpha\rangle$ determined from the fit. Figure 6 shows the values of the pitch angle determined from the (Gaussian) fitted parameters and the values measured directly with a capacitive probe. The agreement throughout the experimental $\langle\alpha\rangle$ range is generally good with perhaps somewhat lower values of the fitted $\langle\alpha\rangle$ at higher experimental $\langle\alpha\rangle$.

The RMS velocity spread values are shown in Fig. 7 for three values of scaled beam current. Parallel velocity spreads are determined from experimental data and the characteristics of the fitted Gaussian. The perpendicular velocity spread is derived using the assumption that the beam electrons are monoenergetic in which case,

$$\frac{\delta v_\perp}{v_\perp} = \frac{1}{\alpha^2} \frac{\delta v_\|}{v_\|} .$$

These are RMS values of spread as compared to the full width at 90% and 10% of the transmitted current as reported by the Soviets[2,13]. Our data suggest that for $\langle\alpha\rangle \geq 0.7$ the perpendicular velocity spreads at a given current are approximately constant and these average spreads increase as a function of beam current from about 7-10% at low beam current to about 15-20% at the largest beam current.

The perpendicular velocity spread in Fig. 8 is shown as a function of the scaled beam current. The experimental points for each current are averages over values of $\langle\alpha\rangle$ greater than about 0.7. Included in the figure is the value from our previous study[7] for the full-voltage, low-current operation scaled to lower current. These values should be compared to the results of a particle trajectory (Herrmannsfeldt) code[14]. This code, or a similar code based on the same equations, was used for the design of the gun, and whose value is shown as the design value in Fig. 8 for a scaled beam current corresponding to $35\,A$. The particle trajectory code includes the external, along with the induced azimuthal magnetic fields, and the macroscopic electrostatic fields. It does not include the self axial magnetic field, two-particle effects, or instability effects. We have also determined (Fig. 9) the perpendicular velocity spread for a $40\,A$ (scaled value of $5\,A$) beam current as a function of velocity ratio. For that part of the $\langle\alpha\rangle$ range near the design value $\langle\alpha\rangle 1.93$, the perpendicular velocity spread is about 5 %. At lower $\langle\alpha\rangle$ values, the spread increase may

result from dramatically different beam optics associated with the indicated $\langle\alpha\rangle$ value and the design value $\langle\alpha\rangle = 1.93$. The experimental behavior is different in both its magnitude and $\langle\alpha\rangle$ dependence. From Fig. 7b, we see that the perpendicular velocity spread increases significantly for $\langle\alpha\rangle \leq 1$.

One result of an increased perpendicular velocity spread is the reflection of some fraction of the beam electrons. Energetically, it is possible for reflected electrons to reach the control anode, and the control anode current was monitored as a function of $\langle\alpha\rangle$ and beam current. Figure 10 shows the control anode current as the beam $\langle\alpha\rangle$ is varied. Also in the figure is the anode current for the high beam current scaled by the ratio of the beam currents. For each beam current value, the current level increases with $\langle\alpha\rangle$; however, at the higher current value, the increase occurs for smaller values of $\langle\alpha\rangle$. Above $\langle\alpha\rangle = 1.5$, the scaled curve is distinctly larger than the $10\,A$ case. This increase is not accounted for by a model of a constant fraction of the beam electrons being reflected at various beam currents. The increase is qualitatively consistent with our measurements of higher velocity spreads at the larger beam current values.

Discussion and Conclusions

The perpendicular velocity spread has been measured in our experiments at modestly scaled operating parameters. The magnitude of the inferred perpendicular velocity spread is much larger than the computational values and in rough agreement with our earlier measurements and measurements made by other groups. In this series of measurements, the values of the average velocity components determined from the retarding potential diagnostic were compared to an independent measurement of the velocity ratio. The close agreement of the two sets of average velocity ratio suggests that the energy diagnostic provides generally reliable results at the scaled operating parameters.

The observed perpendicular RMS velocity spreads for each current level have an approximately constant value for experimental $\langle\alpha\rangle$ above 0.7. And those values of the perpendicular velocity spread increase linearly with beam current, *i.e.* n_e. At the highest equivalent beam current, $40\,A$, the perpendicular velocity spread was $\pm 15 - 20\%$ compared to a computed value of about 5%. This velocity spread is somewhat smaller than the largest values reported by Piosczyk and comparable to the values reported by the Soviets.

A model of the beam electrons reflected by the magnetic hill shows qualitative agreement with current observed on the control-anode. Other electrons may accumulate on other surfaces whose current is not monitored so that the control-anode current is a lower limit to the reflected electron current.

Acknowledgements

Research supported by the Department of Energy Contract DE-AC02-78ET51013 and under appointment to the Magnetic Fusion Science Fellowship program administered by Oak Ridge Associated Universities for the U.S. Department of Energy. Parts of this experimental program were conducted using the facilities at the Francis Bitter National Magnet Laboratory, Cambridge, MA. We also gratefully acknowledge helpful discussions with G. Bekefi and T. Grimm. Assistance in the experimental fabrication was provided by W. Mulligan and G. Yarworth.

References

[1] K.E. Kreischer, T.L. Grimm, W.C. Guss, A.W. Mobius, and R.J. Temkin, Phys. Fluids B **2**,640(1990).

[2] E.G. Avdoshin, L.V. Nikolaev, I.N. Platonov, and Sh. E. Tsimring, Sov. Radiophys. **16**, 461(1973), translation of Izv. VUZ Radiofiz. (USSR) **16**, 605(1973).

[3] E.G. Avdoshin, and A.L. Gol'denberg, Sov. Radiophys. **16**, 36(1974), translation of Izv. VUZ Radiofiz. (USSR) **16**, 1605(1973).

[4] I.I. Antakov, V.A. Gintsburg, E.V. Zasypkin, and E.V. Sokolov, Sov. Radiophys. **18**, 884(1975), translation of Izv. VUZ Radiofiz. (USSR) **18**, 1196(1975).

[5] B. Piosczyk, in *Proceedings of the Seventeenth International Conference on Infrared and Millimeter Waves*, ed. by Richard J. Temkin, SPIE **1929**, 494(1992).

[6] V.E. Zapevalov, Institute of Applied, Nizhny Novgorod, Russian Federation, private communication.

[7] W.C. Guss, T.L. Grimm, K.E. Kreischer, and R.J. Temkin, in *Proceedings of the Fifteenth International Conference on Infrared and Millimeter Waves*, Orlando FL, 1990, edited by R.J. Temkin **SPIE 1514**, 416(1990).

[8] H. Huey, N. Lopez, R. Garcia, and K.E. Kreischer, *Tenth International Conference on Infrared and Millimeter Waves*, p.223 (1985).

[9] K.D. Pearce and W.D. Getty, Bull. Am. Phys. Soc. **36**, 2284(1991).

[10] M. Caulton, RCA Rev. **26**,217(1965).

[11] W.C. Guss, T.L. Grimm, K.E. Kreischer, J.T. Polevoy, and R.J. Temkin, J. Appl. Phys. **69**, 3789(1991).

[12] J. Mark Baird and Wes Lawson, Int. J. Electronics, **61**, 953(1986).

[13] A.L. Gol'denberg, Institute of Applied Physics, Nizhny Novgorod, Russian Federation, private communication.

[14] W.B. Herrmannsfeldt, Electron Trajectory Program, SLAC 226, Stanford Linear Accelerator Center, Stanford, CA 94305, November 1979.

Figure Captions

Fig. 1. Schematic of the gyrotron with source, magnetic field coils and cavity.

Fig. 2. Parallel electron energy analyzer. High voltage is applied to the cylinder and sufficiently energetic electrons reach the collecting electrode.

Fig. 3. The repeller voltage a) and the electrode currents b). The triangles are the net current after the baseline effects have been subtracted.

Fig. 4. Low $\langle\alpha\rangle$ a) and high $\langle\alpha\rangle$ b) swept and pulse-by-pulse data.

Fig. 5. The distribution is determined from the same data by a) a fit to a symmetric Gaussian, and b) taking the derivative of collector electrode characteristic directly.

Fig. 6. Computed $\langle\alpha\rangle$ from the Gaussian fitting process as a function of the experimental $\langle\alpha\rangle$ measured directly by the capacitive probe.

Fig. 7. RMS velocity spreads for the a) parallel and b) perpendicular velocity components for three values of scaled beam current as a function of the experimental $\langle\alpha\rangle$.

Fig. 8. Scaling of perpendicular velocity spread averaged over $\langle\alpha\rangle \geq 0.7$ as a function of the scaled beam current.

Fig. 9. Computed perpendicular velocity spread as a function of $\langle\alpha\rangle$.

Fig. 10. Current collected at the MIG control anode for low ($10\,A$) and high ($40\,A$) beam currents as a function of $\langle\alpha\rangle$. The solid symbols represent the $40\,A$ data scaled to $10\,A$.

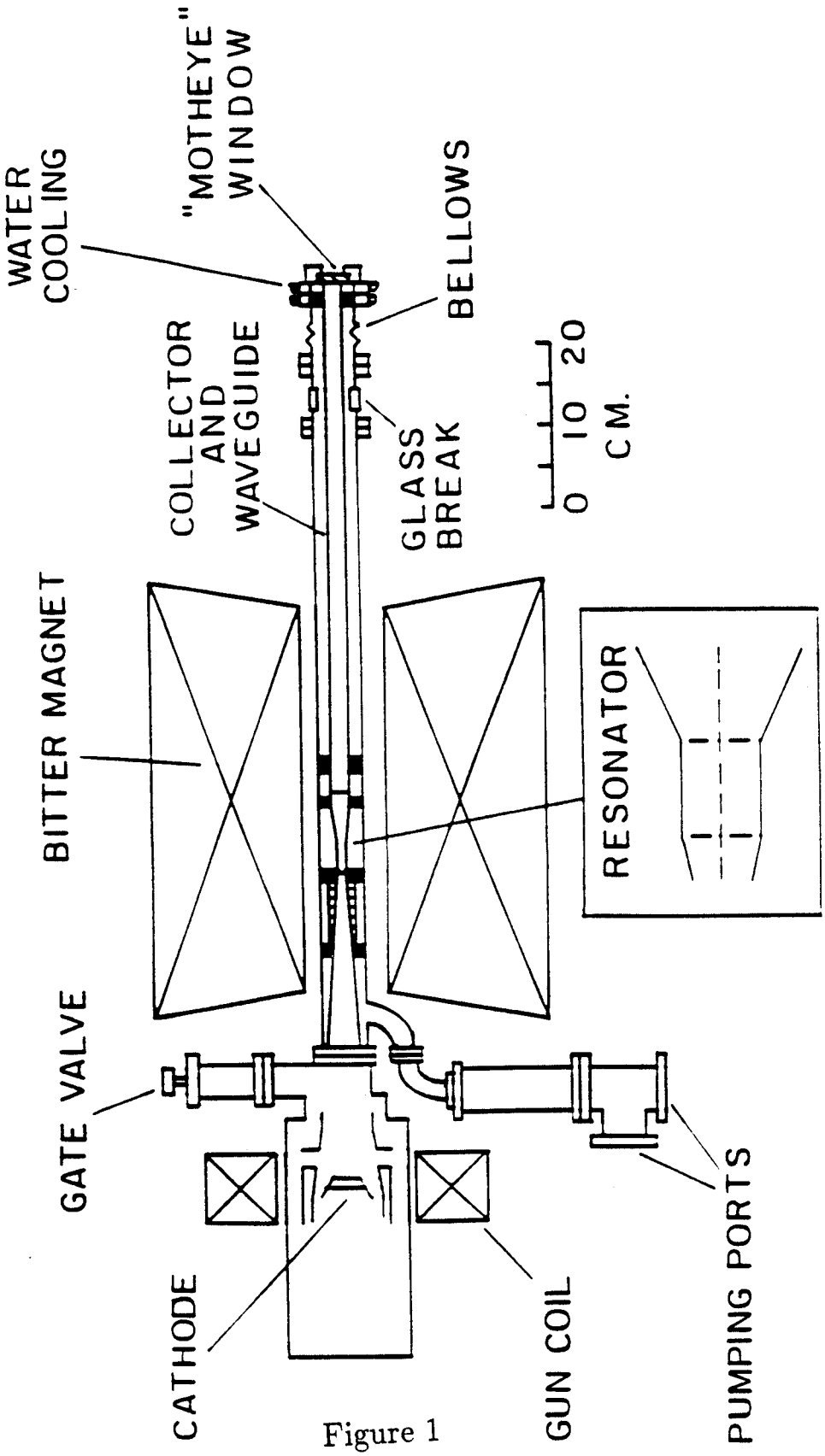
WATER COOLING
"MOTHEYE" WINDOW
BELLOWS
COLLECTOR AND WAVEGUIDE
GLASS BREAK
0 10 20
CM.
BITTER MAGNET
RESONATOR
GATE VALVE
CATHODE
GUN COIL
PUMPING PORTS

Figure 1

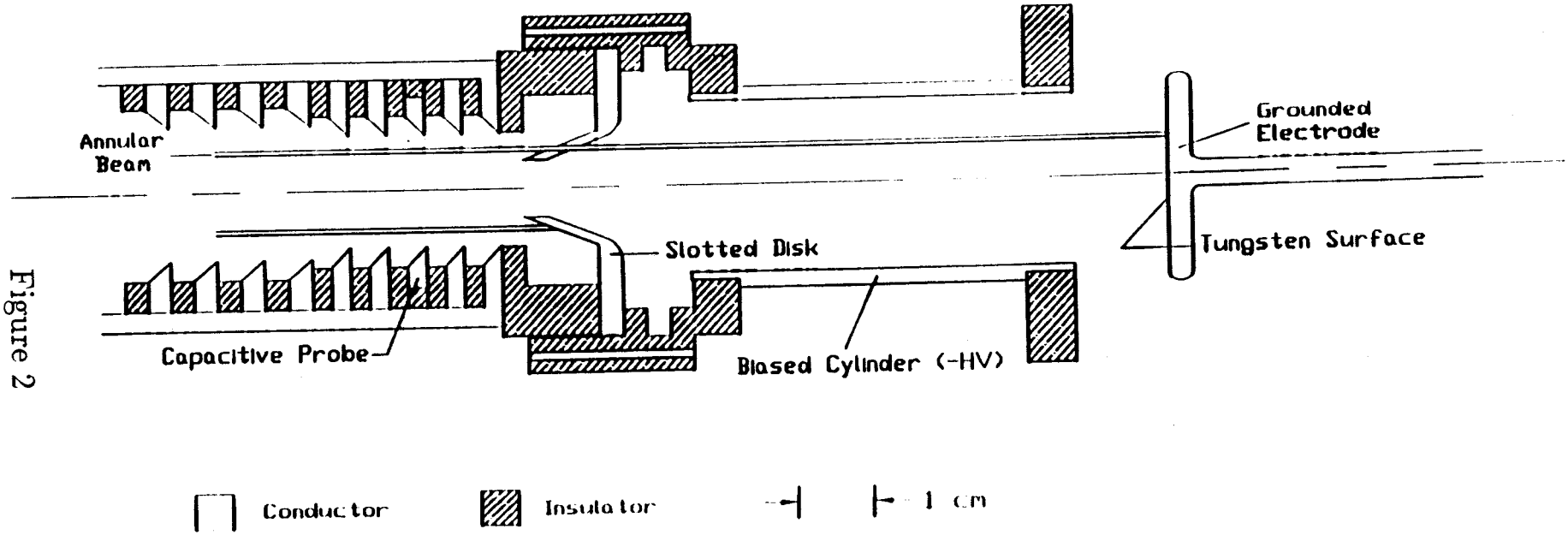
Annular
Beam
Grounded
Electrode
Tungsten Surface
Slotted Disk
Capacitive Probe
Biased Cylinder (-HV)
Conductor
Insulator
1 cm

Figure 2
11

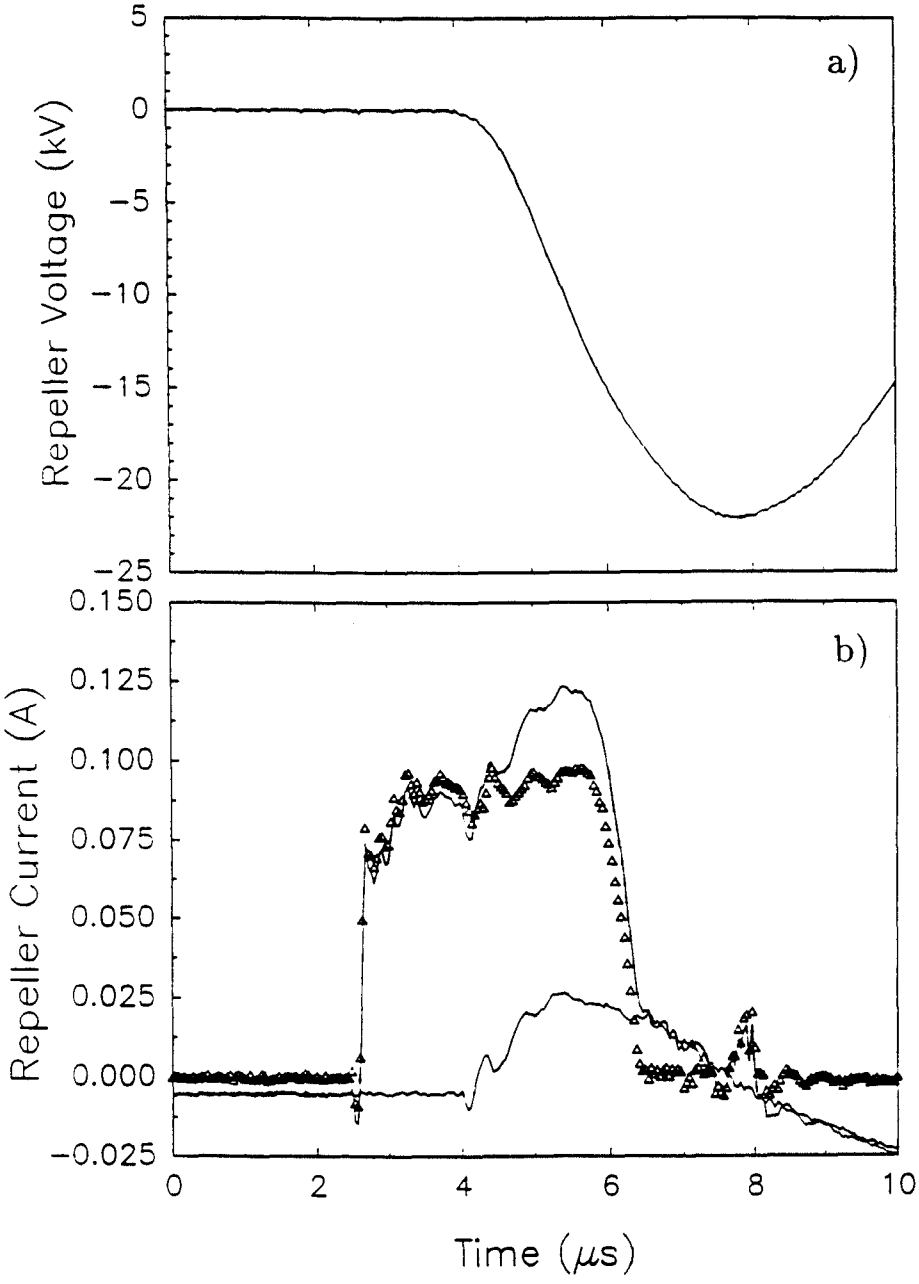
a)
b)
Repeller Voltage (kV)
Repeller Current (A)
Time (μs)
5
0
−5
−10
−15
−20
−25
0.150
0.125
0.100
0.075
0.050
0.025
0.000
−0.025
0
2
4
6
8
10

Figure 3

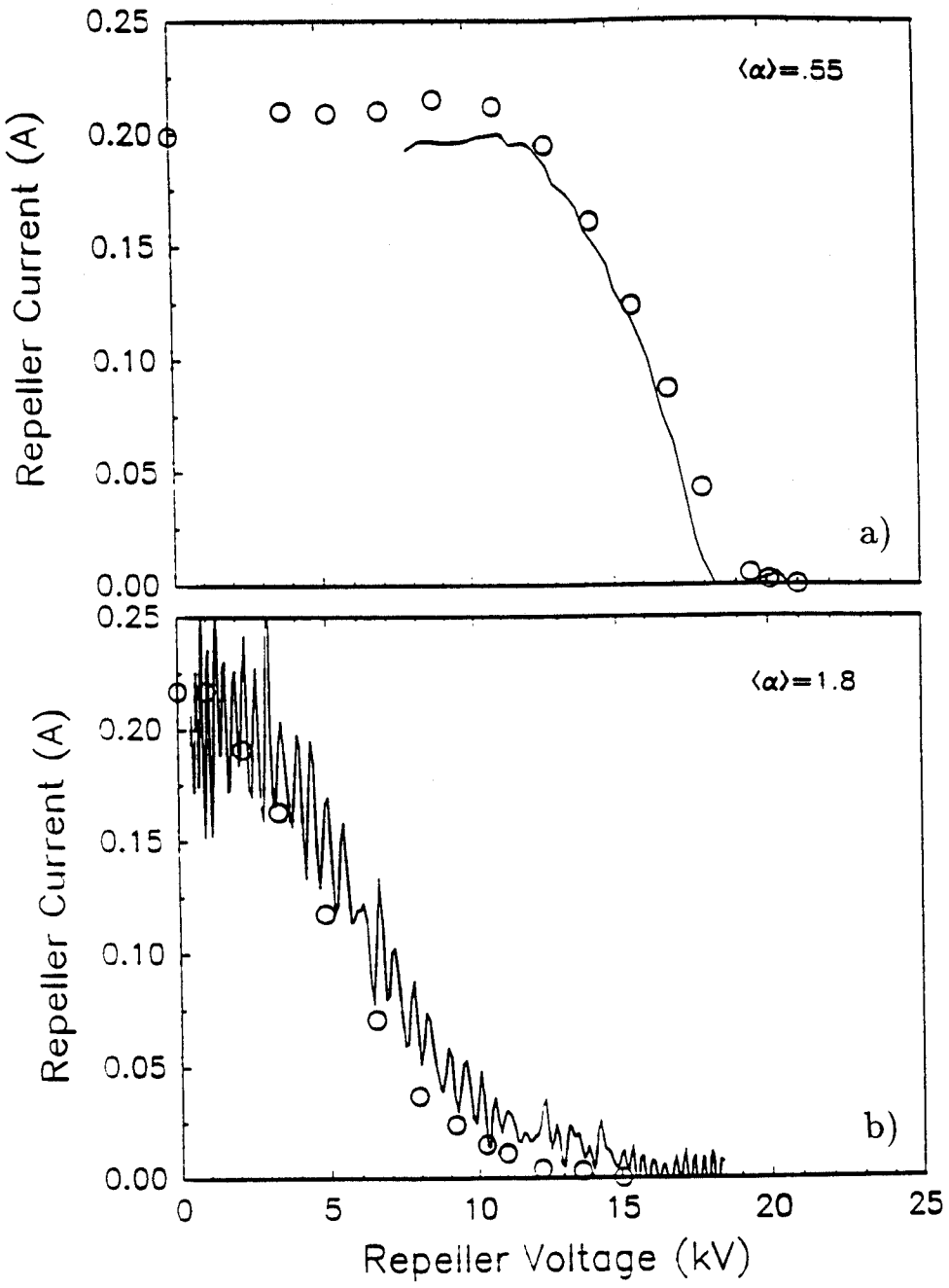
0.25
0.20
0.15
0.10
0.05
0.00
Repeller Current (A)
⟨α⟩=.55
a)
0.25
0.20
0.15
0.10
0.05
0.00
Repeller Current (A)
⟨α⟩=1.8
b)
0
5
10
15
20
25
Repeller Voltage (kV)

Figure 4

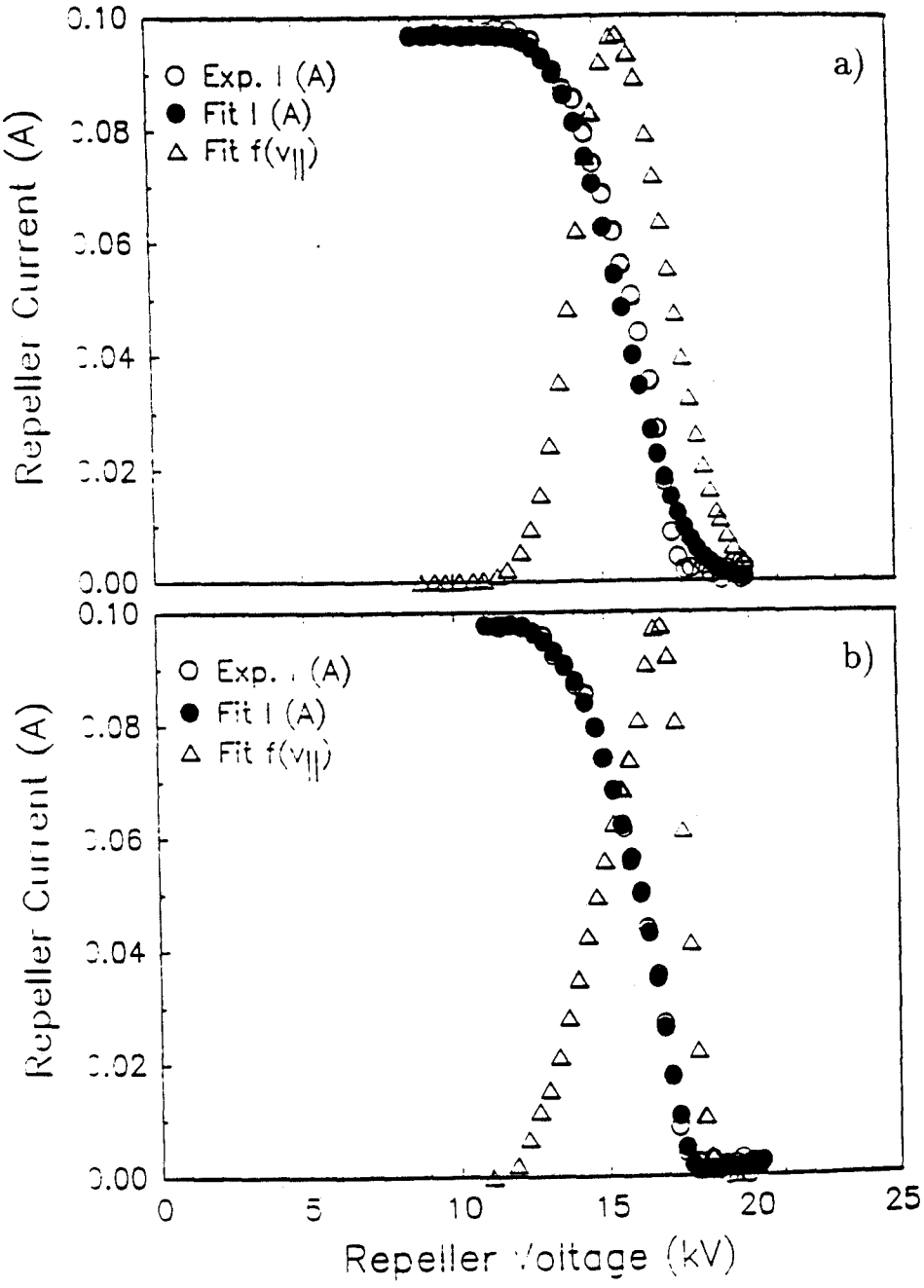
0.10
0.08
0.06
0.04
0.02
0.00
Repeller Current (A)
O Exp. I (A)
● Fit I (A)
△ Fit f(v||)
a)
b)
0
5
10
15
20
25
Repeller Voltage (kV)

Figure 5

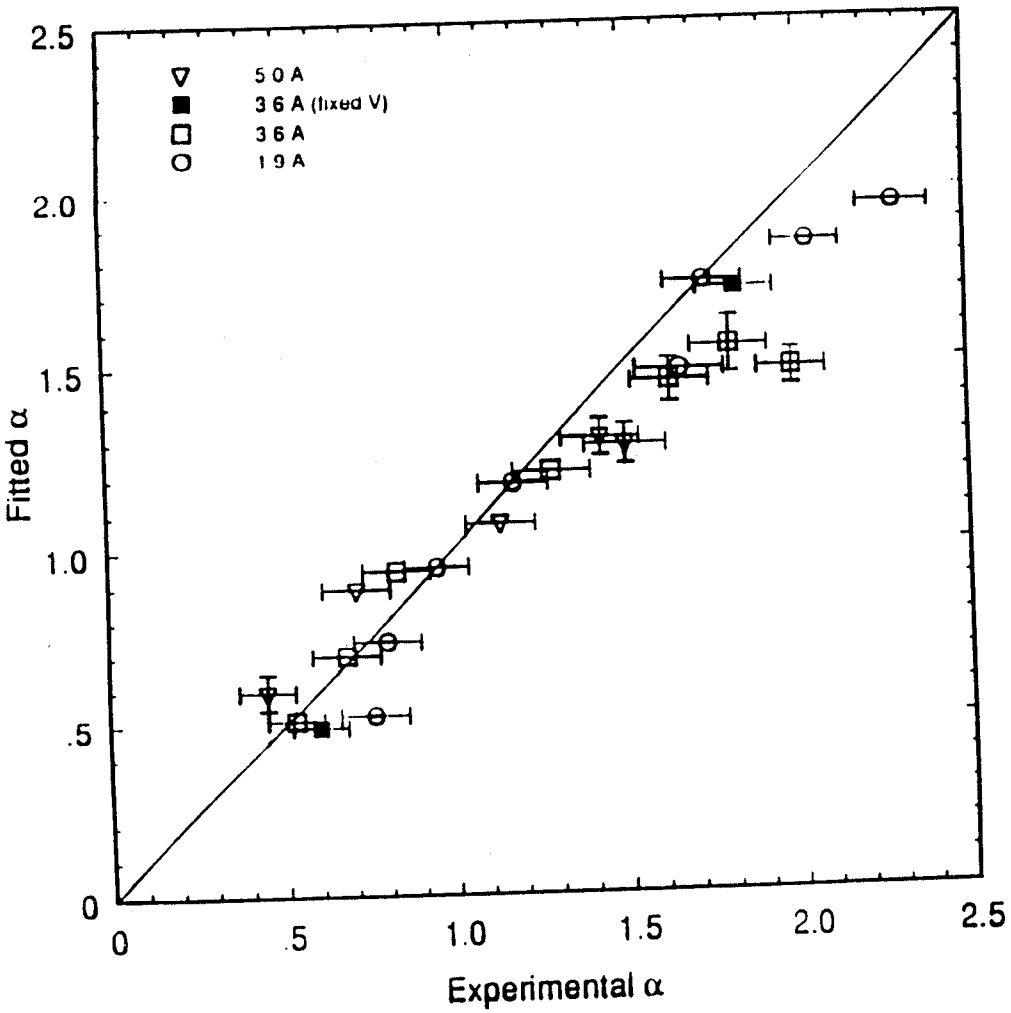

Figure 6

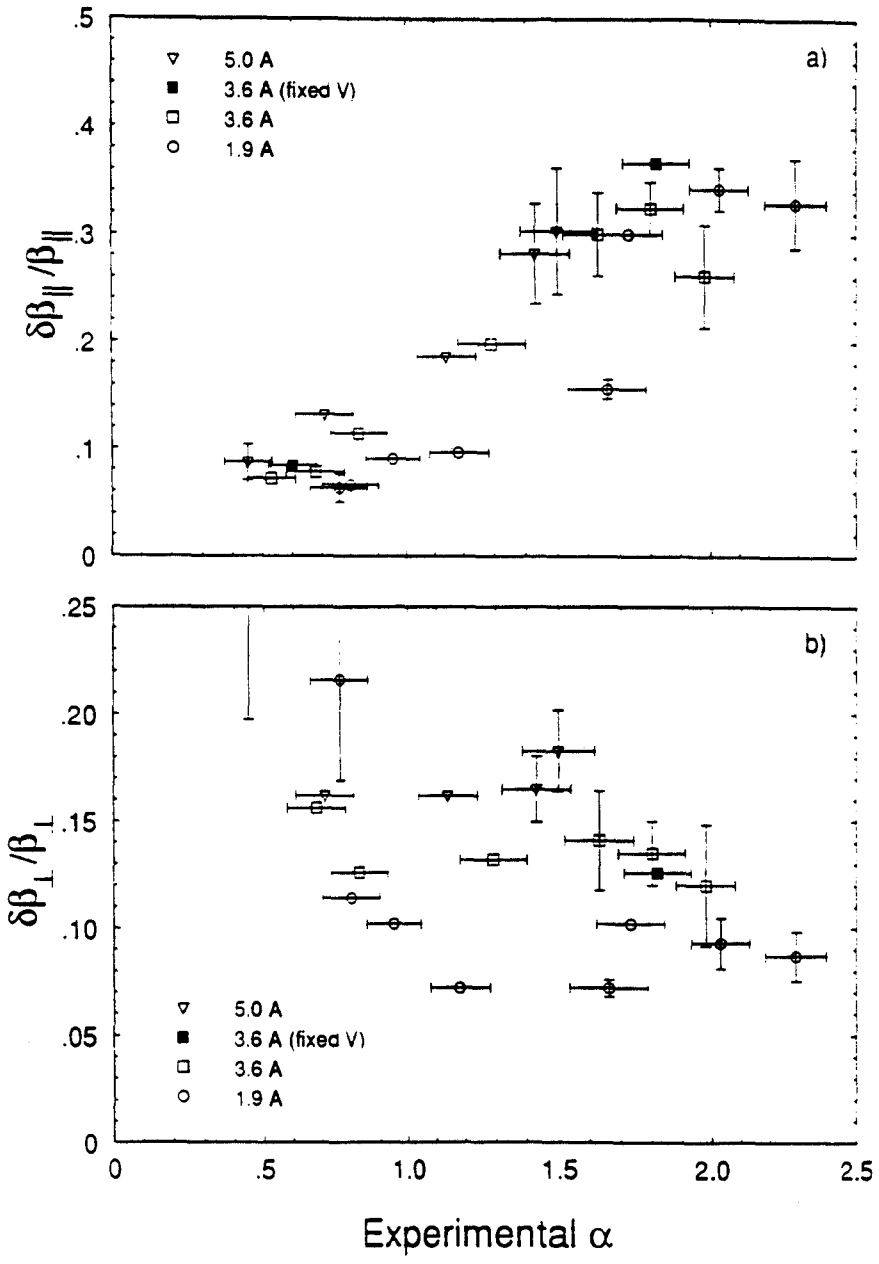
a)
5.0 A
3.6 A (fixed V)
3.6 A
1.9 A
$\delta\beta_{\parallel}/\beta_{\parallel}$
b)
$\delta\beta_{\perp}/\beta_{\perp}$
Experimental α

Figure 7

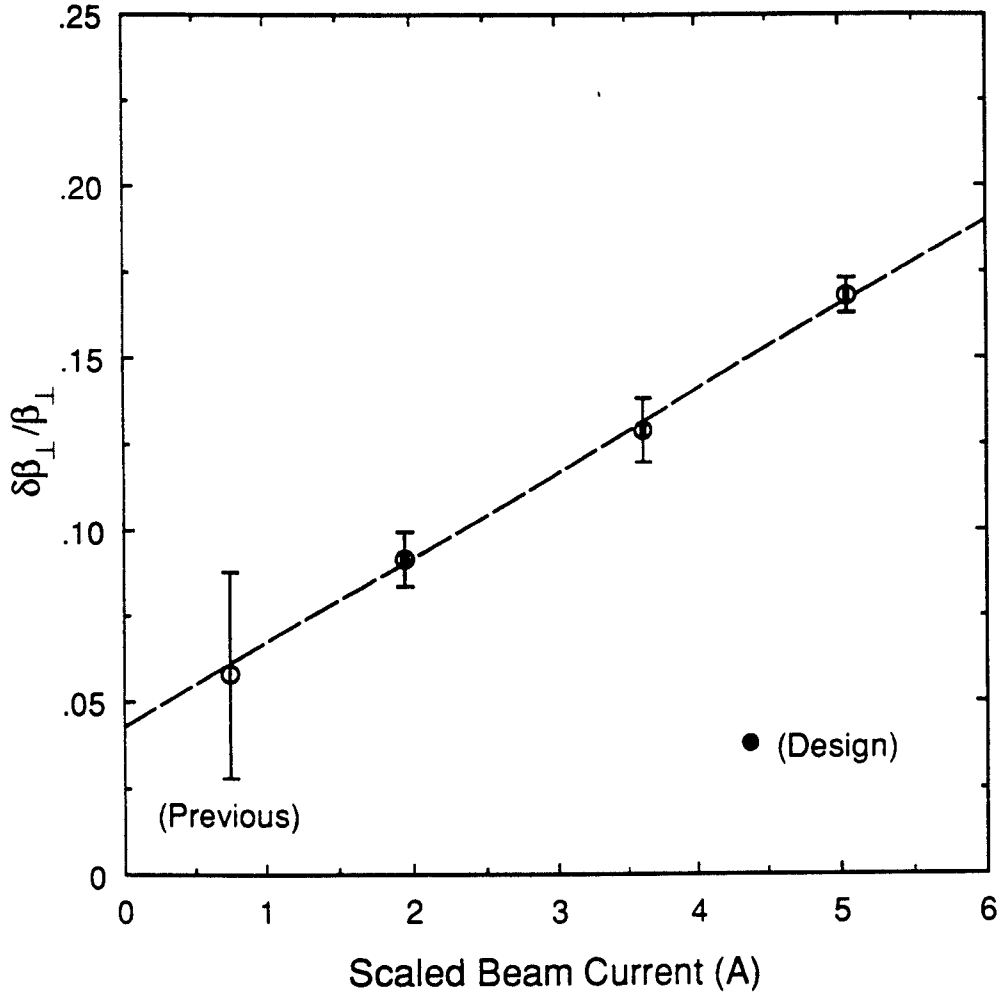
.25
.20
.15
.10
.05
0
$\delta\beta_\perp/\beta_\perp$
0
1
2
3
4
5
6
Scaled Beam Current (A)
(Previous)
(Design)

Figure 8

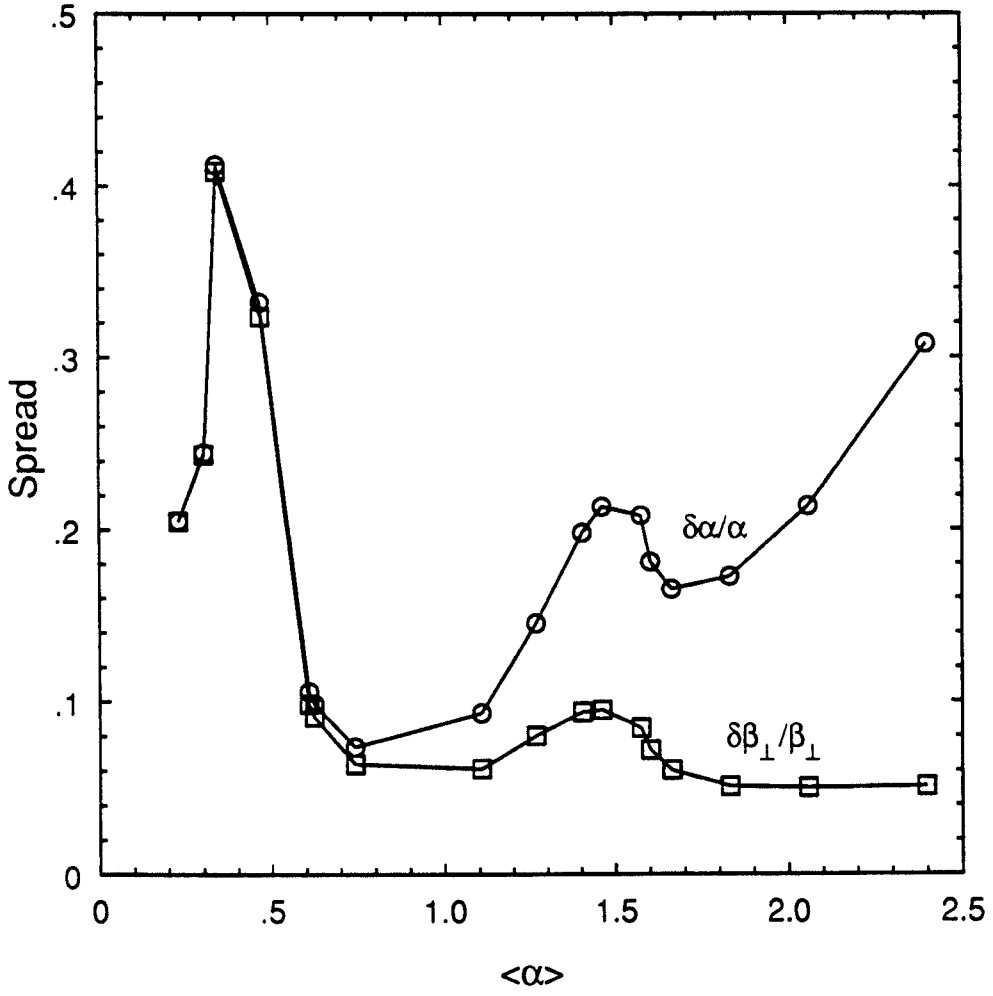

Figure 9

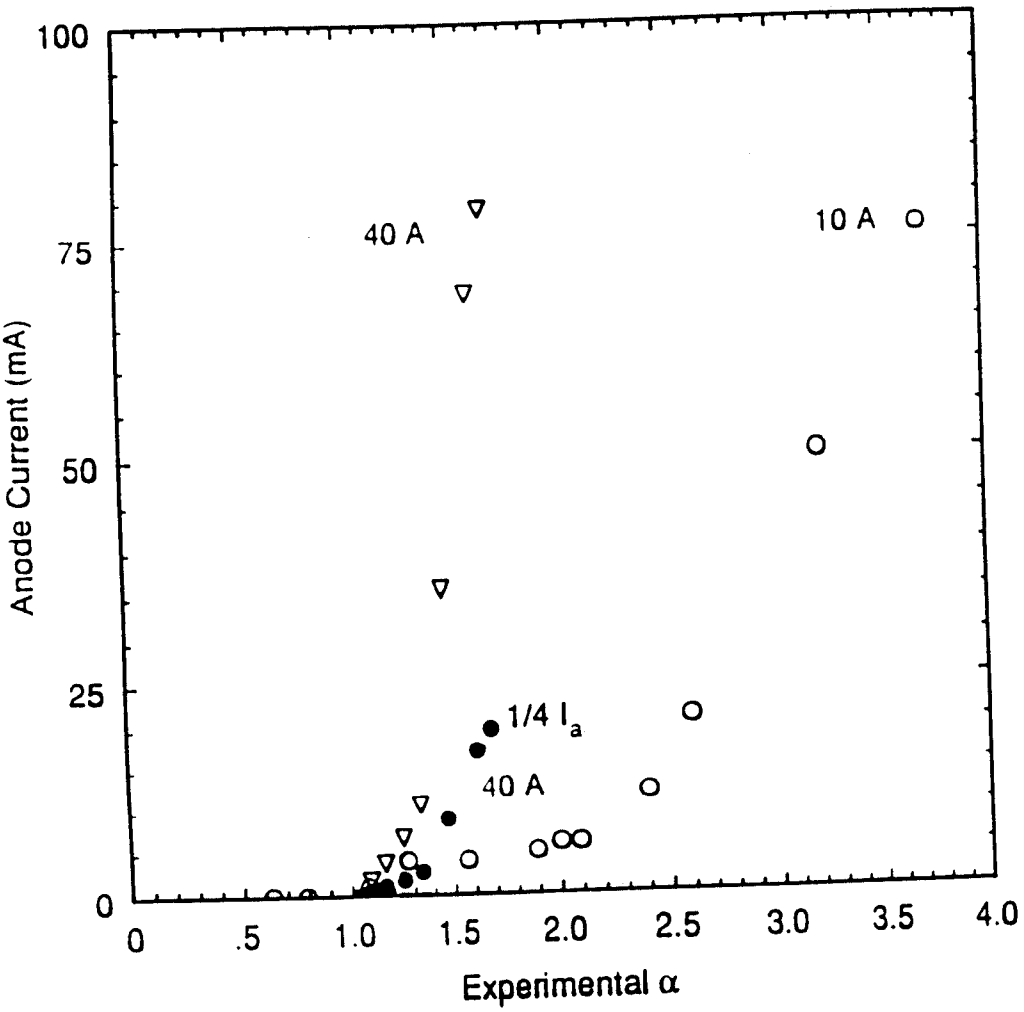
100
75
50
25
0
Anode Current (mA)
40 A
10 A
1/4 I_a
40 A
0
.5
1.0
1.5
2.0
2.5
3.0
3.5
4.0
Experimental α

Figure 10